Research Article

Structural characterization and colour of $Ni_{3-x}Cu_xP_2O_8$ ($0 \le x \le 3$) materials

M. A. Tena[1] · Rafael Mendoza[2] · Camino Trobajo[3] · José R. García[3] · Santiago García-Granda[4]

Received: 14 October 2020 / Accepted: 6 February 2021

Abstract
The structural characterization of $Ni_{3-x}Cu_xP_2O_8$ ($0.0 \le x \le 3.0$) compositions was performed and the colour parameters of these materials measured. Solid solutions with $Ni_3P_2O_8$, $Ni_2CuP_2O_8$ and $Cu_3P_2O_8$ structures were obtained and the compositional range in which they are formed was established. Structural distortion was detected in these solid solutions when x increases from the variation in the unit cell parameters and that of the interatomic distances. Solid solutions with $Ni_3P_2O_8$ structure are stable at 1200 °C and may be used as ceramic pigments. Changes in the colour of these materials were related to the structural changes. Yellow materials are obtained from $Ni_{3-x}Cu_xP_2O_8$ solid solutions with a $Ni_3P_2O_8$ or $Ni_2CuP_2O_8$ structure and a gradual change from yellow to brown is obtained with the introduction of Cu(II) in the $Ni_3P_2O_8$ structure, $0.0 \le x \le 0.7$ at 1200 °C.

Keywords $Ni_3P_2O_8$ · $Ni_2CuP_2O_8$ · $Cu_3P_2O_8$ · Solid solutions · Ceramic pigments

1 Introduction

Metal phosphates can be used to prepare cathode and anode materials, magnetically ordered at low temperature materials and pigments [1–4]. *d*–*d* electronic transitions within transition metal ions give rise to many colours. The absence of a charge transfer band in the visible wavelength range explains the pale blue or weak greenish-blue colourations in $Cu_2P_2O_7$ and $Cu_3P_2O_8$ compounds. Strong absorbance due to charge transfers is the most important component in the colouration of some materials [4–6]. The Ni(II) orthophosphate structure is stable with temperature and in a commercial glaze and can be used as a yellow ceramic pigment in industry [4]. The $Ni_3P_2O_8$ compound melts at 1350 °C. Yellow colouration can be also stable in some commercial glazes or can change to beige in others commercial glazes. Dopant cations and changes in the structure of the compounds modify their physical properties. Phosphates have a high capacity to form solid solutions. For example, $Mg_{0.5}Cu_{1.5}V_xP_{2-x}O_7$ ($0 < x \le 2$) solid solutions fired at 600 °C can be used in the preparation of yellow–orange–red paint pigments. The colour of the materials darkens with increasing temperature [6].

Information about $Ni_3P_2O_8$, $CuNi_2P_2O_8$ and $Cu_3P_2O_8$ compounds can be found in the bibliography but information about solid solutions between $Ni_3P_2O_8$—$Cu_3P_2O_8$ compositions cannot be found. At 900 °C, mixtures of the $Cu_3P_2O_8$ and $CuNi_2P_2O_8$ or $Ni_3P_2O_8$ and $CuNi_2P_2O_8$

Supplementary information The online version contains supplementary material available at https://doi.org/10.1007/s42452-021-04348-3.

✉ M. A. Tena, tena@uji.es; Rafael Mendoza, mendozarafael@uniovi.es; Camino Trobajo, ctf@uniovi.es; José R. García, jrgm@uniovi.es; Santiago García-Granda, s.garciagranda@cinn.es | [1]Inorganic Chemistry Area, Inorganic and Organic Chemistry Department, Jaume I University, P.O. Box 224, Castellón, Spain. [2]Physical Chemistry Area, Scientific and Technical Services, Oviedo University-CINN, Oviedo, Spain. [3]Inorganic Chemistry Area, Organic and Inorganic Chemistry Department, Oviedo University-CINN, Oviedo, Spain. [4]Physical Chemistry Area, Physical and Analytical Chemistry Department, Oviedo University-CINN, Oviedo, Spain.

Published online: 25 February 2021

crystalline phases are obtained from $Cu_{3-x}Ni_xP_2O_8$ compositions when the content in Cu(II) or Ni(II) is high [7]. Information about the stability of these compounds and mixtures of compounds with the temperature is not included.

$Ni_3P_2O_8$ crystallizes in the monoclinic system with space group P 1 2_1/c 1, $a = 5.830(2)$ Å, $b = 4.700(2)$ Å, $c = 10.107(4)$ Å, $\beta = 91.22(2)°$ and $Z = 2$ [8]. In the $Ni_3P_2O_8$ crystal structure the Ni(II) ions are octahedrally coordinated at two types of sites: a special site (2a) and a general site (4e), with average Ni–O bond lengths of 2.081(2) Å and 2.067(2) Å. Groups of three octahedra (Ni_3O_{14} edge-sharing octahedra) are interconnected with tetrahedra PO_4. The phosphorus atoms occupy only one crystallographic site (4e). The mean P–O bond length is 1.547(2) Å, although the tetrahedron shows some unusually large distortions with bond lengths ranging from 1.521(2) to 1.595(2) Å. Four different sites are occupied by oxygen atoms (four 4e general positions) in this structure. Figure 1 shows the $Ni_3P_2O_8$ structure from ICSD-153159 data [9]. The structure was drawn with the Studio program [10–12]. Yellow lines have been drawn between the oxygen atoms in a group of three octahedra and all the atoms in this trimer have been labelled. This compound exhibits three-dimensional antiferromagnetic couplings with a Neel temperature of 17.1 K and it is magnetically ordered at 1.5 K. It is an antiferromagnetic phase with the presence of ferromagnetic couplings in the trimer units [3].

The only Ni(II) and Cu(II) orthophosphate structure described to date corresponds to the 2:1:2:8 stoichiometry. $Ni_2CuP_2O_8$ crystallizes in the monoclinic $P2_1/n$ space group, with cell parameters $a = 6.393(1)$ Å, $b = 9.325(1)$ Å, and $c = 4.718(1)$ Å; $\beta = 90.71(1)$; $V = 281.24$ Å^3; and $Z = 2$ [9], standard cell 4.7180, 9.3250, 7.8983, 90.000, 125.967, 90.000 (space group P 1 $2_1/c$ 1). The Cu(II) ions are in CuO_4 planar square coordination (Cu1 at a special site (2a)) with an average Cu–O bond length of 1.990(2) Å. The Ni(II) ions are in square-planar pyramid coordination (Ni1 at a general site (4e)) with an average Ni–O bond length of 2.031(2) Å. Each two square-planar pyramids have two common oxygen atoms (Ni_2O_8 dimers) and are linked to CuO_4 planar squares by one oxygen atom. The Ni_2O_8 dimers and CuO_4 planar squares form chains connected with tetrahedra PO_4. The phosphorus atoms occupy only one crystallographic site (4e). The mean P-O bond length being 1.538(2) Å with bond lengths ranging from 1.5055(2) Å to 1.5552(2) Å. Four different sites (four general positions

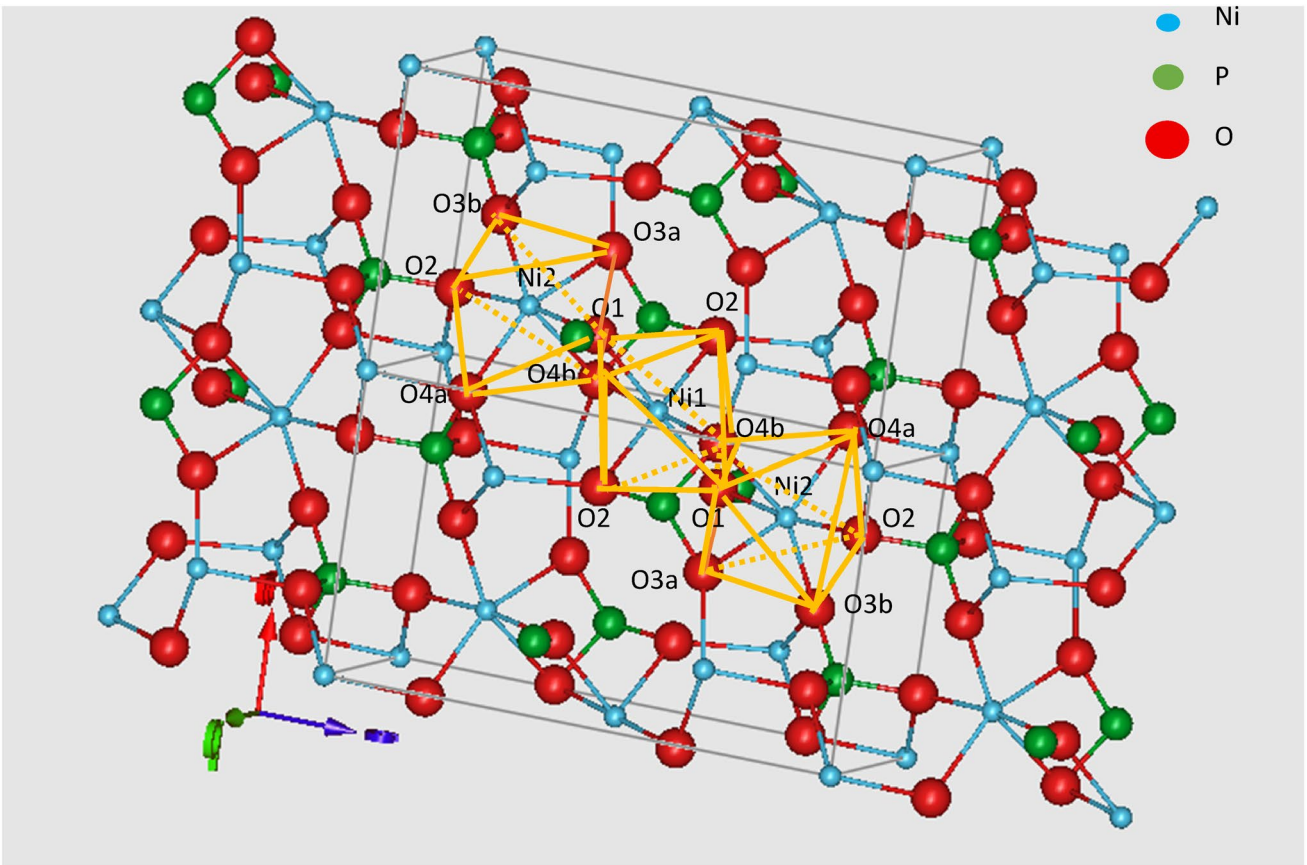

Fig. 1 The crystal structure of $Ni_3P_2O_8$ with the labelled atoms for a Ni2-Ni1-Ni2 trimer. Axes: **a**, in red; **b**, in green; and **c**, in blue

(4e)) are occupied by oxygen atoms in this structure. Figure 2 shows the crystal structure of $Ni_2CuP_2O_8$ with the labelled atoms for a planar square centred around Cu and a Ni_2O_8 dimer obtained from ICSD-245202 data [9]. The structure was drawn with the Studio program [10–12]. Yellow lines have been drawn between the oxygen atoms in a part of the -CuO_4-Ni_2O_8-CuO_4-Ni_2O_8- chain. The heterometallic phosphate $Ni_2CuP_2O_8$ was obtained from the thermal treatment of the Cu(II) intercalated compound [13]. The $Ni_2CuP_2O_8$ phosphate has also been synthesized via the ceramic method at 800 °C in air [14]. This compound exhibits three-dimensional antiferromagnetic couplings with a Neel temperature of 29.8 K and it is magnetically ordered at 2.0 K temperature. It is an antiferromagnetic phase with the presence of ferromagnetic couplings inside the Ni_2O_8 dimers [13, 14].

$Cu_3P_2O_8$ crystallizes in the triclinic system with space group $P-1$, $a=4.8537(7)$ Å, $b=5.2855(6)$ Å, $c=6.1821(8)$ Å, $\alpha=72.35(1)°$, $\beta=86.99(1)°$, $\gamma=68.54(1)°$ and $Z=1$ [15]. The Cu(II) ions are in planar squares coordination (Cu1 in CuO_4) and square-planar pyramids coordination (Cu2 in CuO_5) at two types of sites: a special site (1a) and a general site (2i), with average Cu–O bond lengths of 1.949(2) and 2.030(2) Å. Each two square-planar pyramids have two common oxygen atoms (Cu_2O_8 dimers) and are linked to CuO_4 planar squares by one oxygen atom. Copper-oxygen layers are formed by zig-zag chains (–CuO_4–CuO_5–CuO_5–CuO_4–) which form four- and six-membered rings, the chains being aligned parallel to the [101] direction [15]. Only one crystallographic site is occupied by phosphorus atoms (2i), which are tetrahedrally coordinated with oxygen atoms. The mean P-O bond length is 1.540(2) Å, with bond lengths ranging from 1.510(2) to 1.572(2) Å (the tetrahedron distortions in $Cu_3P_2O_8$ are smaller than in $Ni_3P_2O_8$). Four different sites (four general positions (2i)) are occupied by oxygen atoms in the $Cu_3P_2O_8$ structure [9]. Figure 3 shows the crystal structure of $Cu_3P_2O_8$ with the labelled atoms for a planar square centred around Cu1 (CuO_4) and a Cu_2O_8 dimer obtained from ICSD-68811 data [9]. The structure was drawn with the Studio program [10–12]. Yellow lines have been drawn between the oxygen atoms in a part of the –CuO_4–Cu_2O_8–CuO_4–Cu_2O_8– chain (repeating group). This compound orders antiferromagnetically at $T_N=22$ K [16].

Ni (II) ions are octahedrally coordinated in the $Ni_3P_2O_8$ structure and in square-planar pyramidal coordination in the $Ni_2CuP_2O_8$ structure while Cu (II) ions are in planar square coordination in $Ni_2CuP_2O_8$ and $Cu_3P_2O_8$ structures and in square-planar pyramidal coordination in the structure $Cu_3P_2O_8$. Therefore, the coordination of square-planar pyramids can be occupied by Ni (II) and Cu (II) ions and these ions could be substituted in the formation of possible solid solutions.

The aim of this study was to investigate the possible formation of $Ni_{3-x}Cu_xP_2O_8$ ($0.0 \le x \le 3.0$) solid solutions with $Ni_3P_2O_8$, $Ni_2CuP_2O_8$ and $Cu_3P_2O_8$ structures so as to

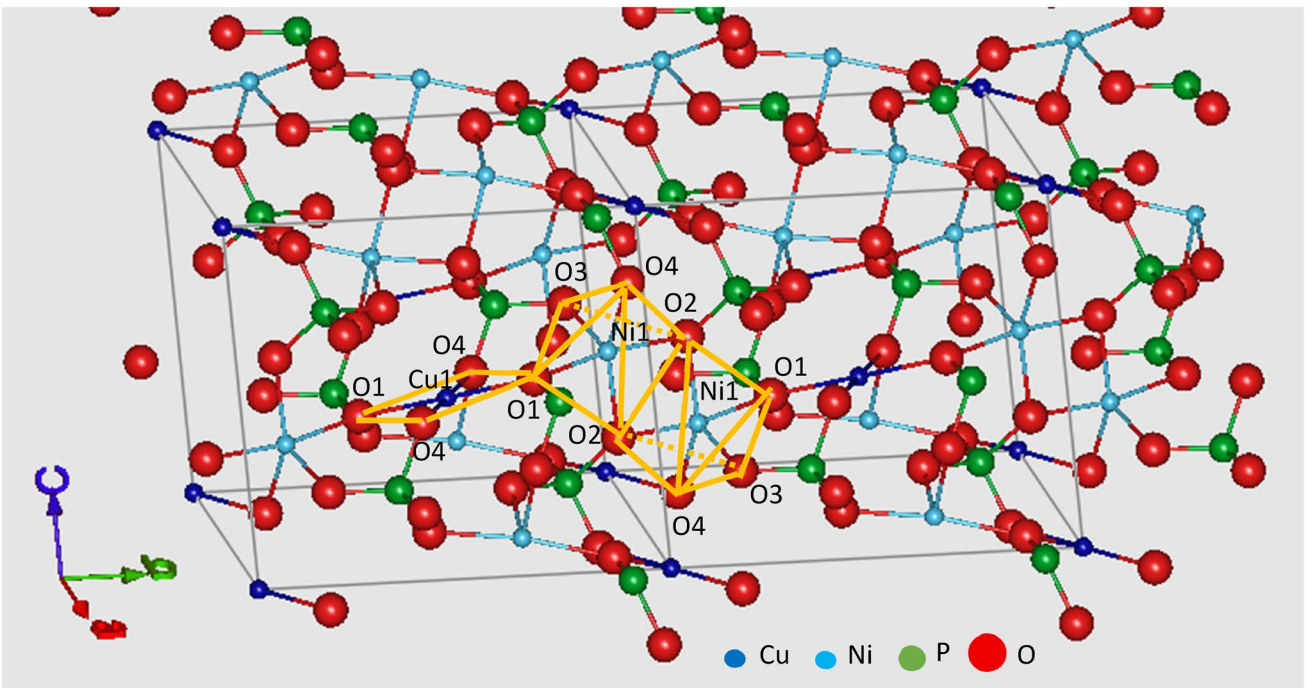

Fig. 2 The crystal structure of $Ni_2CuP_2O_8$ with the labelled atoms for a group repeating on the –CuO_4–Ni_2O_8–CuO_4–Ni_2O_8– chains. Axes: a, in red; b, in green; and *c*, in blue

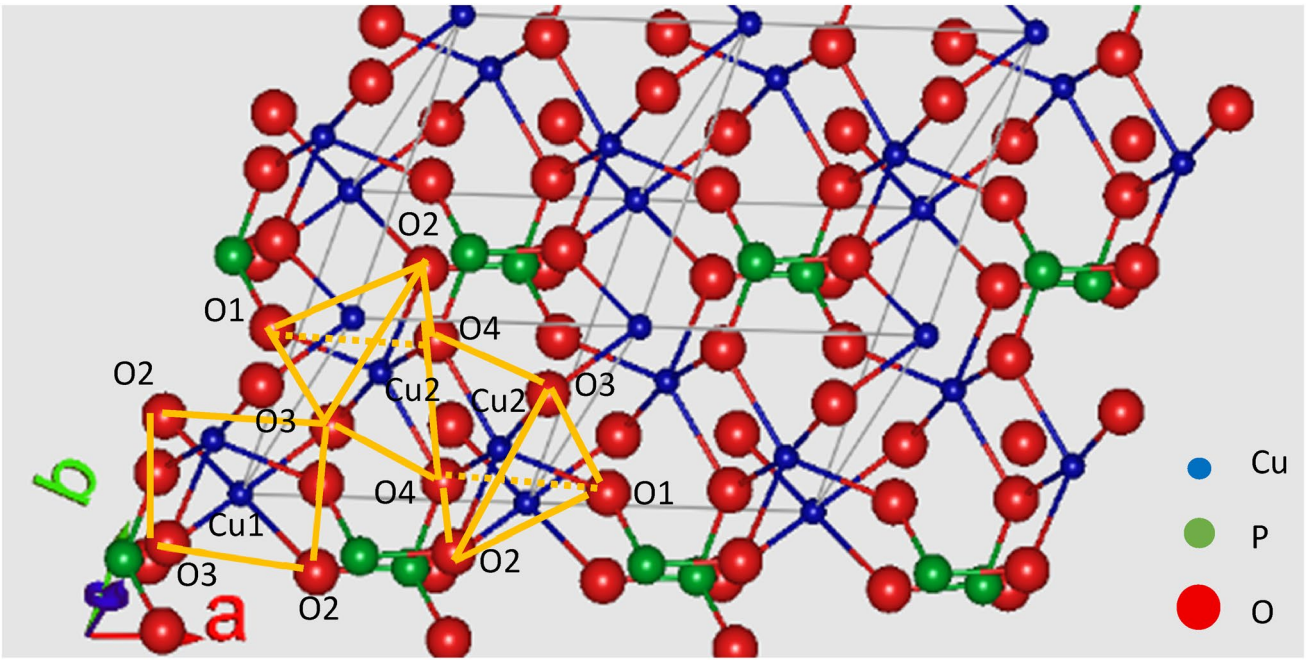

Fig. 3 The crystal structure of $Cu_3P_2O_8$ with the labelled atoms for a planar square (CuO_4) and a Cu_2O_8 dimer, repeating group on the zig-zag chains. Axes: a, in red; b, in green; and c, in blue

establish the compositional limits they present and monitor the evolution of the colour of these materials with composition and temperature for the purpose of obtaining materials with different shades of yellow or brown that may be used as ceramic pigments.

2 Experimental

$Ni(NO_3)_2{\cdot}6H_2O$ (Acros Organic, 99%), $Cu(NO_3)_2{\cdot}2.5\ H_2O$ (Sigma-Aldrich, 98%) and H_3PO_4 (Merck, 99%) were used to synthesize $Ni_{3-x}Cu_xP_2O_8$ ($0.0 \le x \le 3.0$) compositions via the chemical co-precipitation method. The stoichiometric amount of $Ni(NO_3)_2{\cdot}6H_2O$, $Cu(NO_3)_2{\cdot}2.5\ H_2O$ and a 0.5 M solution of H_3PO_4 in water were added to water to obtain a final volume of 200 mL. Samples were vigorously stirred for 12 h at room temperature and then an ammonia aqueous solution (Panreac, 25%) was added until reaching pH 10. The materials co-precipitated were dried using IR-irradiation until to obtain the 100% in solid materials. The Ni:Cu:P molar ratio of the starting materials is preserved. Only water is evacuated with drying. The dry samples were fired at 300, 600, 800, 1000 and 1200 °C for 6 h at each temperature.

To study the development of the crystalline phases at different temperatures, the resulting materials were examined using a Panalytical X-ray diffractometer with CuK_α radiation. Diffraction patterns ranging between 6 and 110° (2θ) were collected employing monochromatic CuK_α radiation, a step size of 0.02° (2θ) and a sampling time of 10 s. Fullprof.2 k computer program based on the Rietveld method [10–12] was used to refine the structures by adjusting the diffraction profile. The unit cell parameters and interatomic distances in the developed structures were obtained to investigate the possible formation of solid solutions under these synthesis conditions. The initial structural information was obtained from the Inorganic Crystal Structure Database [9]. This database includes standard cell [17], standard space group, fractional atomic coordinates and other information on crystalline phases found in the literature.

The Ni(II) and Cu(II) sites and the transfer charge bands in the materials were studied by UV–Vis-NIR spectroscopy (diffuse reflectance). A Jasco V-670 spectrophotometer was used to obtain the ultraviolet visible near infrared (UV–Vis-NIR) spectra in the 200 to 2500 nm range.

The CIEL*a*b* colour parameters on the fired compositions were obtained with an X-Rite spectrophotometer (SP60, standard illuminant D65, an observer 10°, and a reference sample of MgO). L* is the lightness axis (black (0) → white (100)), a* is the green (–) → red (+) axis, and b* is the blue (–) → yellow (+) axis [18].

3 Results and discussion

Table 1 shows the evolution of the crystalline phases with composition and temperature in the $Ni_{3-x}Cu_xP_2O_8$ ($0.0 \le x \le 3.0$) samples. At 600 °C, the $Ni_3P_2O_8$ composition is not crystalline under the synthesis conditions employed in this study. The $Ni_3P_2O_8$ crystalline phase can be detected with a weak or medium diffraction intensity when $0.5 \le x \le 2.5$ at this temperature. At temperatures above 600 °C, the $Ni_3P_2O_8$ crystalline phase is developed only when $x \le 1.0$. At 600 °C, the $Ni_2CuP_2O_8$ phase can be detected when $1.5 \le x \le 2.5$. At temperatures above 600 °C, this phase is detected in all compositions including Ni(II) and Cu(II), $0.5 \le x \le 2.5$, and it is the only crystalline phase when $1.5 \le x \le 2.0$ at 800 °C and when $x = 0.20$ at 1000 °C. The $Cu_3P_2O_8$ crystalline phase can be detected with medium and strong diffraction intensities in compositions when $1.5 \le x \le 3.0$ at 600 °C. At temperatures above 600 °C, the $Cu_3P_2O_8$ crystalline phase is detected when $x \ge 2.5$. At 1200 °C, $x \ge 1.5$ compositions melt and the diffraction intensities show strong preferred orientations. When $1.5 \le x \le 2.0$, a crystalline phase $M_3P_2O_8$ (M = Ni, Cu) with $Z = 4$ and S.G. $P-1$ (structure type "triclinic $Mg_3P_2O_8$" (ICSD-84710)), develops at 1200 °C under the experimental conditions employed in this study. The coordination number of M is 4, 5 and 6 in this last structure. The evolution of the crystalline phases with temperature from $x = 1.0$ composition ($Ni_2CuP_2O_8$) is shown in Fig. 4.

Table 2 shows the unit cell parameters in the $Ni_3P_2O_8$ structure obtained from $Ni_{3-x}Cu_xP_2O_8$ ($0.0 \le x \le 1.0$) fired compositions, while the values at 800, 1000 and 1200 °C are represented in Fig. 5. The slight increase in the a unit cell parameter of the $Ni_3P_2O_8$ structure with increasing x is in accordance with the partial substitution of Ni(II) by Cu(II), as the radius of Cu(II) is slightly larger than that of Ni(II). No significant variation in the b unit cell parameter is observed and the decrease in the *c* unit cell parameter is not according with the ionic radius. These inverse variations of the a and *c* parameters can be attributed to the deformation of the $Ni_3P_2O_8$ structure when Cu(II) is incorporated and the increase in the unit cell volume is very slight (Table 3). This structure is not compact throughout its volume; it includes less dense areas that allow this deformation. From Fig. 5, the $x = 0.7$ composition can be established as the composition with the maximal distortion in the $Ni_3P_2O_8$ structure and this composition is seen to be the limit composition in the formation of solid solutions with this structure. At 800–1200 °C, $Ni_{3-x}Cu_xP_2O_8$ solid solutions are formed when $x \le 0.7$.

The inverse variation in the *a* and *b* parameters in the $Ni_2CuP_2O_8$ structure were obtained from the $Ni_{3-x}Cu_xP_2O_8$ ($1.5 \le x \le 2.5$) compositions fired at 800 and 1000 °C (Table 4 and Fig. 6). As the radius of Cu(II) is slightly larger than that of Ni(II), the increase in the a unit cell parameter is in accordance with the partial substitution of Ni(II) by Cu(II), but the decrease in *b* cannot be explained by the radius values. The aforementioned increase can be explained by the deformation of the $Ni_2CuP_2O_8$ structure when Cu(II) is incorporated, forming solid solutions. Hence, the increase in the unit cell volume is very slight (Table 3). The variation in the c parameter is the smallest and the β angle increases with *x*. A composition limit with *x* cannot be established from Fig. 6. The variation in the unit cell parameters is more evident when $x \ge 1.0$ and the $Ni_{3-x}Cu_xP_2O_8$ solid solutions with a $Ni_2CuP_2O_8$ structure may well have been formed when $1.0 \le x \le 2.5$ at 800 and 1000 °C.

In the $Cu_3P_2O_8$ structure, structural deformation was obtained with decreasing x (Table 5). A slight decrease in the a and b unit cell parameters of the $Cu_3P_2O_8$ structure with decreasing x is in accordance with the partial substitution of Cu(II) by Ni(II), as the radius of Ni(II) is slightly smaller than that of Cu(II). The slight increase in the c unit

Table 1 Evolution of crystalline phases with temperature in $Ni_{3-x}Cu_xP_2O_8$ compositions (XRD patterns of the samples are included in the supporting information)

x	600 °C	800 °C	1000 °C	1200 °C
0.0	–-	N(s)	N(s)	N(s)
0.5	N(vw)	N(s), C(m)	N(s), C(vw)	N(s), C(vw)
1.0	N(w)	C(s), NP(m)	C(s), N(w)	N(s), C(vw),
1.5	N(m), P(m), A(m), C(w)	C(s)	C(s), CP(vw)	X(s)
2.0	P(s), C(m), A(w), N(w), B(vw)	C(s)	C(s)	X(s), C(w)
2.5	P(s), C(m), A(vw), B(vw), N(vw)	P(s), C(m)	P(s), C(m)	C(s), P(m)
3.0	P(s), A(m), B(vw)	P(s)	P(s)	P(s)

Crystalline phases: N = $Ni_3P_2O_8$ (monoclinic, P 1 2_1/c 1), C = $Ni_2CuP_2O_8$ (monoclinic, P 1 2_1/c 1), P = $Cu_3P_2O_8$ (Z = 1, triclinic, P -1), A = α-$Cu_2P_2O_7$ (monoclinic, C 1 2/c 1), B = β-$Cu_2P_2O_7$ (monoclinic, C 1 2/m 1), X = $M_3P_2O_8$ (M = Cu, Ni; Z = 4; triclinic, P -1; "$Mg_3P_2O_8$-triclinic")

Diffraction peak intensity: s = strong, m = medium, w = weak, vw = very weak

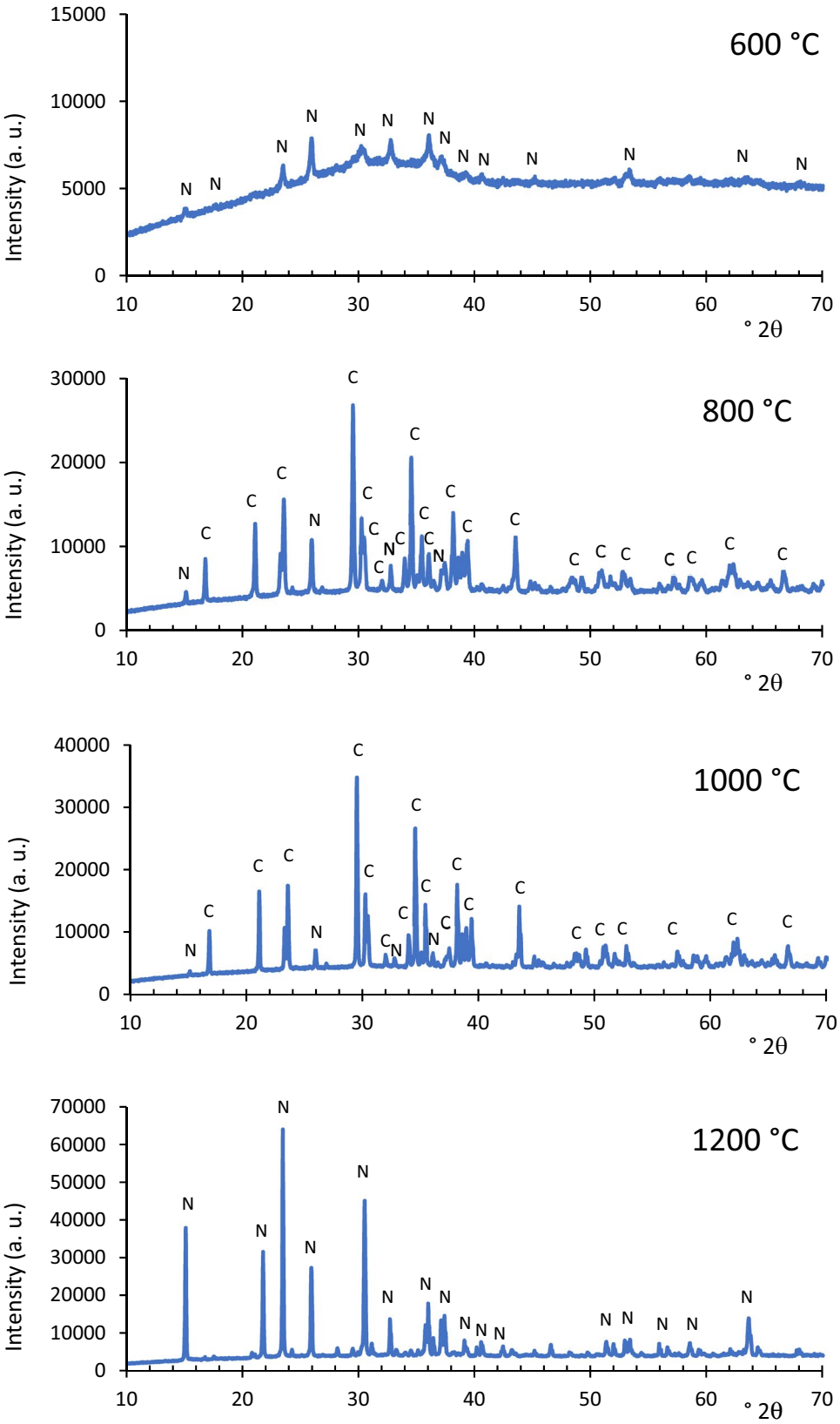

Fig. 4 Crystalline phases obtained from the $Ni_2CuP_2O_8$ composition ($x = 1.0$). N = $Ni_3P_2O_8$, C = $Ni_2CuP_2O_8$

Table 2 Variation in unit cell parameters in the $Ni_3P_2O_8$ structure obtained from $Ni_{3-x}Cu_xP_2O_8$ fired compositions

T (°C)	x	*a* (Å)	*b* (Å)	*c* (Å)	*β* (°)
600	1.0	5.87 (6)	4.70 (5)	10.06 (11)	91.2 (8)
600	1.5	5.8699 (5)	4.6979 (4)	10.0505 (8)	90.973 (6)
800	0.0	5.82696 (8)	4.69654 (8)	10.1053 (1)	91.1244 (9)
800	0.5	5.84946 (9)	4.69672 (9)	10.0880 (2)	91.073 (1)
800	1.0	5.8513 (2)	4.6960 (2)	10.089 (4)	91.043 (3)
1000	0.0	5.82673 (5)	4.69607 (4)	10.10529 (8)	91.1320 (5)
1000	0.5	5.86013 (6)	4.69620 (6)	10.0776 (1)	91.0473 (8)
1000	1.0	5.8575 (1)	4.6964 (1)	10.0815 (2)	91.0472 (9)
1200	0.0	5.82625 (5)	4.69474 (4)	10.10279 (8)	91.1272 (6)
1200	0.5	5.8485 (1)	4.6953 (1)	10.0832 (2)	91.088 (1)
1200	1.0	5.8472 (1)	4.6955 (1)	10.0844 (2)	91.109 (2)

cell parameter is not in accordance with the ionic radius. At 600 °C, a tendency for the volume of this structure to decrease with *x* can be detected in the $3.0 \geq x \geq 1.5$ compositional range (Table 3). At $T > 600$ °C, the $Cu_3P_2O_8$ structure is developed in the compositions with $x \geq 2.5$.

Figure 7 shows the variation in the M–O and P–O distances in the $Ni_3P_2O_8$ structure. This variation is in accordance with the variation in the unit cell parameters (Fig. 5). The increase in the M2–O3b and M2-O4b distances with increasing amounts of Cu(II) ions ($0 \leq x \leq 0.7$) lengthens the a unit cell parameter because the Ni2–O4b direction is near to that of the a axis. The Ni1–O and Ni2–O distances and the position of the labelled atoms for a Ni2–Ni1–Ni2 trimer are shown in Fig. 1. The O1–M2–O2 direction is parallel to the *c* axis and the decrease in the M2–O1 and M2–O2 distances shortens the *c* unit cell parameter with increasing *x*. The O4b–M1–O4b direction is near to the direction of the *c* axis and the slight decrease in the M1–O4b distance contributes to the decrease in the c unit cell parameter. An increase in the covalent component in the M1–O4b bonds in the *c* direction might explain this variation, which is not in accordance with the variation in the ionic radius. The longest M2–O4a distance (the O4a oxygen atoms are bonded to two trimers) does not vary with *x*. The variation in the obtained distances could be explained by the tendency to square plane coordination of Cu(II), a plane of the octahedron with smaller distances and the other two oxygen atoms situated at a longer distance. The $Ni_2CuP_2O_8$ and $Cu_3P_2O_8$ structures with Cu(II) in square plane coordination are obtained when $x \geq 1.0$ at 1000 °C (Table 1). No significant change in the three similar P–O distances around 1.54 Å and a slight increase in the four distances around 1.60 Å are detected at 1000 °C.

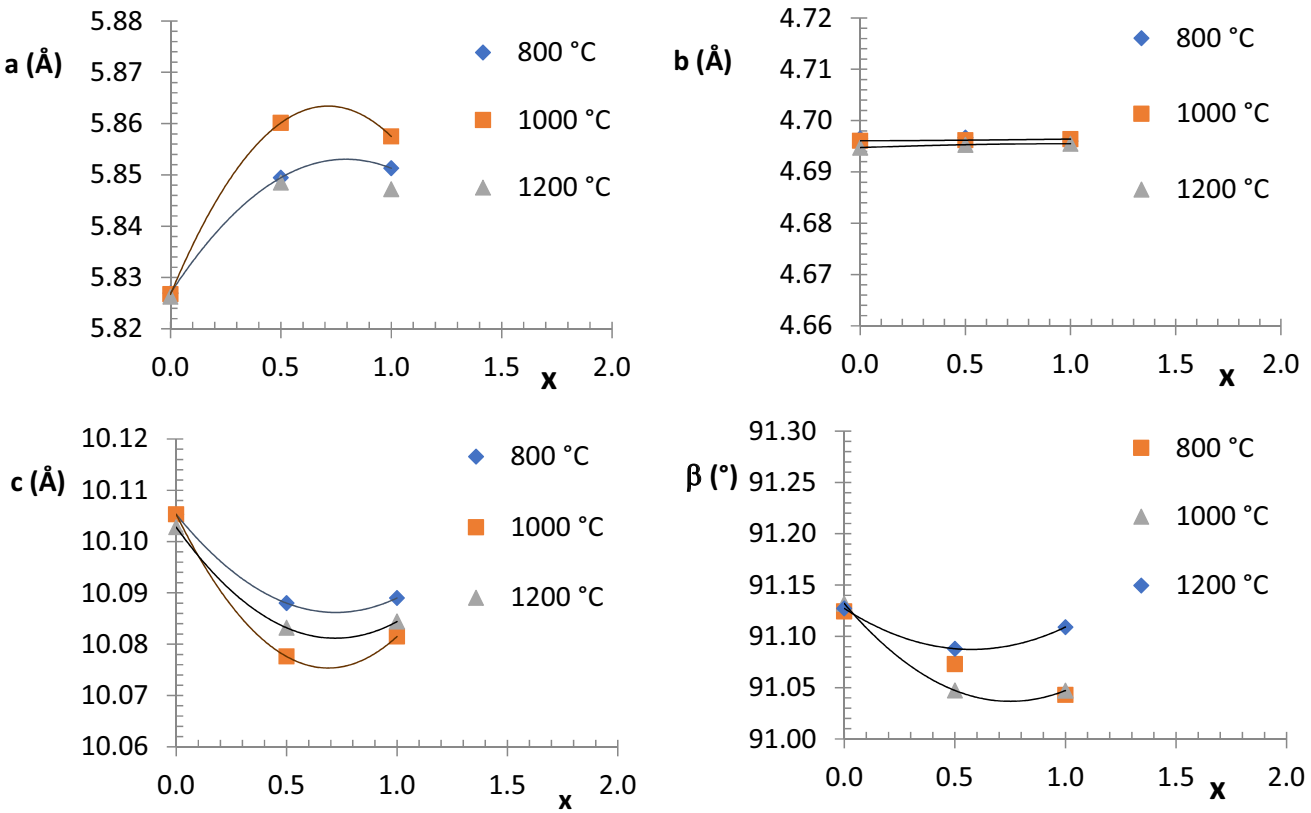

Fig. 5 Variation in unit cell parameters in the $Ni_3P_2O_8$ structure obtained from $Ni_{3-x}Cu_xP_2O_8$ compositions fired at 800, 1000 and 1200 °C

Table 3 Variation in unit cell volume in $Ni_3P_2O_8$, $Ni_2CuP_2O_8$ and $Cu_3P_2O_8$ structures obtained from $Ni_{3-x}Cu_xP_2O_8$ fired compositions

T (°C)	*x*	$Ni_3P_2O_8$ V (Å^3)	$Ni_2CuP_2O_8$ V (Å^3)	$Cu_3P_2O_8$ *V* (Å^3)
600	1.5	277.12 (4)	–	134.68 (3)
600	2.0	–	–	135.23 (2)
600	2.5	–	–	140.56 (1)
600	3.0	–	–	140.483 (8)
800	0.0	276.494 (7)	–	–
800	0.5	277.101 (8)	281.30 (1)	–
800	1.0	277.18 (2)	281.425 (8)	–
800	1.5	–	281.442 (6)	–
800	2.0	–	281.354 (7)	–
800	2.5	–	281.30 (1)	140.533(6)
800	3.0	–	–	140.484(3)
1000	0.0	276.455 (4)	–	–
1000	0.5	277.293 (5)	281.30 (1)	–
1000	1.0	277.286 (7)	281.425 (8)	–
1000	1.5	–	281.442 (6)	–
1000	2.0	–	281.354 (7)	–
1000	2.5	–	281.30 (1)	140.533 (6)
1000	3.0	–	–	140.460 (4)
1200	0.0	276.285 (4)	–	–
1200	0.5	276.84 (1)	281.10 (3)	–
1200	1.0	276.824 (9)	281.0 (1)	–
1200	2.5	–	281.37 (1)	140.514 (5)
1200	3.0	–	–	140.584 (7)

Table 4 Variation in unit cell parameters in the $Ni_2CuP_2O_8$ structure (std cell) obtained from $Ni_{3-x}Cu_xP_2O_8$ fired compositions

T (°C)	*x*	*a* (Å)	*b* (Å)	*c* (Å)	*β* (°)
800	0.5	4.7220 (1)	9.3139 (2)	7.9054 (2)	125.993 (1)
800	1.0	4.71871 (7)	9.3251 (1)	7.9018 (1)	125.9645 (9)
800	1.5	4.72594 (5)	9.3173 (1)	7.90170 (9)	126.0122 (6)
800	2.0	4.75108 (6)	9.2808 (1)	7.9043 (1)	126.1718 (8)
800	2.5	4.7625 (1)	9.2610 (3)	7.9060 (2)	126.227 (2)
1000	0.5	4.7220 (1)	9.3103 (3)	7.9028 (2)	125.986 (2)
1000	1.0	4.71555 (4)	9.32634 (8)	7.90163 (7)	125.9508 (5)
1000	1.5	4.72312 (6)	9.3202 (1)	7.8978 (1)	125.9881 (7)
1000	2.0	4.75043 (5)	9.2816 (1)	7.90365 (8)	126.1770 (5)
1000	2.5	4.75964 (9)	9.2681 (2)	7.9048 (2)	126.229 (1)
1200	0.5	4.7148 (3)	9.3242 (5)	7.9013 (4)	125.975 (4)
1200	2.5	4.75797 (9)	9.2721 (6)	7.9038 (2)	126.201 (2)

From the variation in the M(II)–O bond lengths (M = Ni, Cu) with x in the $Ni_2CuP_2O_8$ structure at 1000 °C (Fig. 8), a decrease in most of the bonds and an increase in the M1-O4 and M2-O3 (M1 = Cu, M2 = Cu, Ni) distances can be observed. These last bonds are aligned in the direction of the a axis (Fig. 2) and their increase with increasing amounts of Cu(II) ions ($1.0 \le x \le 2.5$) lengthens the a unit cell parameter (Fig. 6). This increase is in accordance with the partial substitution of the Ni(II) ion by the slightly larger Cu(II) ion. All the other M–O distances decrease when x increases. This decrease causes a decrease in the b unit cell parameter and may be due to the increased covalent character of the bond when the increasing amount of Cu(II) ions in the compositions is replaced by Ni(II) ions. Deformation of the tetrahedra around the P atoms is detected in this structure with increasing *x*. The P–O3 distance (O3 is coordinated to P and M2) decreases and the P-O1 distance (O1 is coordinated to P, Cu1 and M2) increases with x.

The presence of Ni(II) in the $Cu_3P_2O_8$ structure decreases the M2–O2 and M1–O3 distances (M2–O2 is considerably longer than the other distances) and increase the other distances with decreasing *x* (there is Ni(II) in the compositions). It is in accordance with the decrease in the *a* and *b* parameters and the increase in the *c* unit cell parameter when *x* decreases (Table 5 and Fig. 3). This phase is only developed when $x \ge 2.5$ at $T > 600$ °C. The presence of Ni(II) weakens most of the bonds while strengthening the longest bond. Hence, distortion occurs with the formation of solid solutions in the three structures to accommodate the cations.

Figure 9 shows the UV–V spectra obtained from the $Ni_3P_2O_8$ and $Cu_3P_2O_8$ compositions (raw material and fired composition). Three absorption bands assigned to Ni^{2+} at an octahedral site are detected from $Ni_3P_2O_8$ fired at $T \ge 800$ °C. Maximum values of these bands are observed around 1300 nm ($^3A_{2g} \rightarrow {}^3T_{2g}$(F), first transition), 800 nm ($^3A_{2g} \rightarrow {}^3T_{1g}$(F), second transition) and 450 nm ($^3A_{2g} \rightarrow {}^3T_{1g}$(P), third transition). The [200–650] wavelength range includes the absorption band associated with the third d-d transition and the charge transfer band of Ni(II)–O. The three spin-allowed transitions of Ni^{2+} at an octahedral site generally fall within the 1400–800, 900–500 and 550–370 nm ranges, respectively, in octahedral systems [19]. The broad band observed in $Cu_3P_2O_8$ fired at $T \ge 800$ °C within the 550–1900 nm wavelength range with the absorption maximum at 800–900 nm is assigned to the d-d transition of the Cu^{2+} ion (d^9). A *d–d* transition is allowed from the Cu(II) ion. At 1200 °C, the charge transfer band of Cu(II)–O is observed around 400 nm. The high asymmetry observed in all the bands is due to the difference in Ni–O (between 1.982 and 2.181 Å) and Cu–O distances (between 1.924 and 2.259 Å) in the $Ni_3P_2O_8$ and $Cu_3P_2O_8$ structures (ICSD-153159 and ICSD-1143 [5]). Structural distortion due to the Jahn–Teller effect also contributes to the asymmetry in the observed bands obtained from the $Cu_3P_2O_8$ composition.

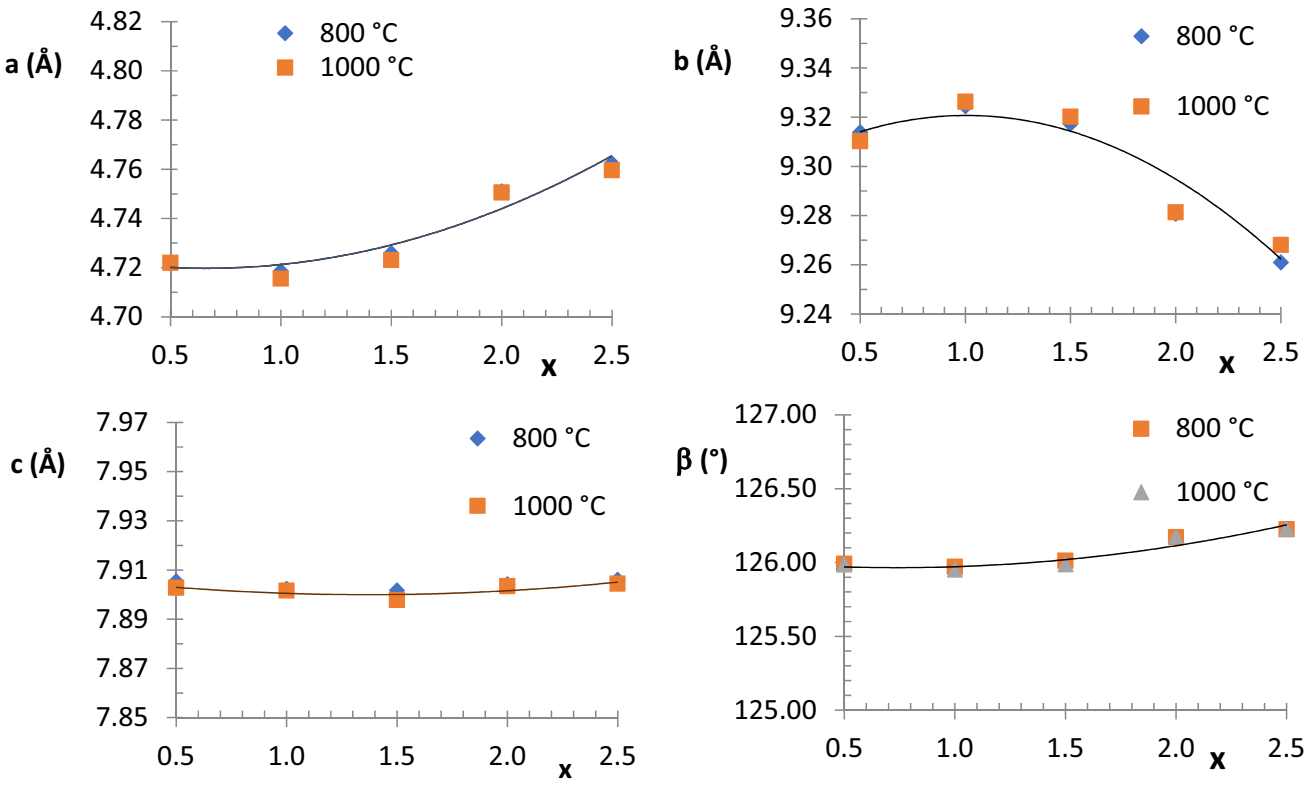

Fig. 6 Variation in unit cell parameters in the $Ni_2CuP_2O_8$ structure obtained from $Ni_{3-x}Cu_xP_2O_8$ compositions fired at 800 and 1000 °C

Table 5 Variation in unit cell parameters in the $Cu_3P_2O_8$ structure obtained from $Ni_{3-x}Cu_xP_2O_8$ fired compositions

T (°C)	*x*	*a* (Å)	*b* (Å)	*c* (Å)	*α* (°)	*β* (°)	*ϒ* (°)
800	2.5	4.8479 (1)	5.2788 (1)	6.2056 (2)	72.354 (2)	87.002 (2)	68.533 (2)
800	3.0	4.85561 (7)	5.28732 (8)	6.18340 (9)	72.3845 (8)	87.022 (1)	68.5196 (8)
1000	2.5	4.84291 (6)	5.27645 (6)	6.21425 (7)	72.3152 (8)	86.9769 (9)	68.5502 (7)
1000	3.0	4.85467 (5)	5.28713 (6)	6.18472 (6)	72.3378 (9)	86.994 (1)	68.5310 (8)
1200	2.5	4.84557 (9)	5.2780 (1)	6.2087 (1)	72.327 (1)	86.991 (2)	68.556 (1)
1200	3.0	4.8569 (2)	5.2895 (2)	6.18444 (5)	72.335 (1)	86.985 (2)	68.534 (3)

The UV-V spectra obtained from the $Ni_{3-x}Cu_xP_2O_8$ ($0.0 \le x \le 3.0$) compositions fired at 800, 1000 and 1200 °C are shown in the Fig. 10. The three absorption bands assigned to Ni^{2+} at an octahedral site and the d-d transition band of the Cu^{2+} ion can be observed when $x \le 2.0$ and $x \ge 2.5$, respectively. Slight variations are observed with the change in the Ni^{2+}:Cu^{2+} ratio. An increase in absorbance around 1700 nm can be detected. In the $Ni_3P_2O_8$ composition, a shoulder in the band assigned to the first Ni(II) transition band appears at this wavelength. The maximum value of this band is not observed around 1300 nm in $1.5 \le x \le 2.0$ compositions at 800 °C. At this temperature, the variation with composition in the inflection point between maximum and minimum absorbance within the 650–1000 nm wavelength range (second Ni(II) transition band) can be observed in $0.0 \le x \le 2.0$ compositions. The wavelength at these inflection points increases with the amount of copper in the samples (*x*). No noticeable changes in the position of the Ni(II) third transition with x can be detected. These slight changes in spectra with composition are related to the variation in the Ni–O and Cu–O distances, which involve changes in the relative position of the oxygen atoms around M(II) (M = Ni, Cu) with x in the crystalline phases detected by XRD. With increasing temperature, the increase in absorbance around 1100 nm makes it

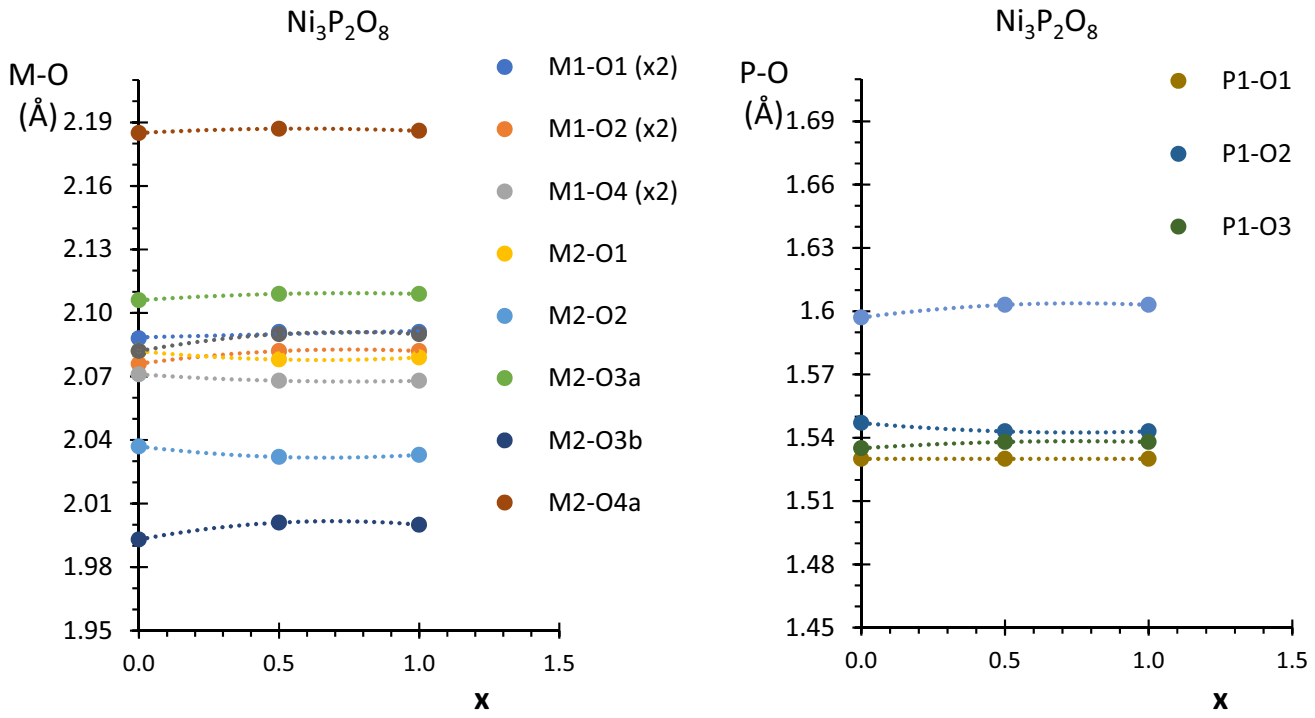

Fig. 7 Variation in interatomic distances in the $Ni_3P_2O_8$ structure obtained from $Ni_{3-x}Cu_xP_2O_8$ compositions fired at 1000 °C

Fig. 8 Variation in interatomic distances in the $Ni_2CuP_2O_8$ structure obtained from $Ni_{3-x}Cu_xP_2O_8$ compositions fired at 1000 °C

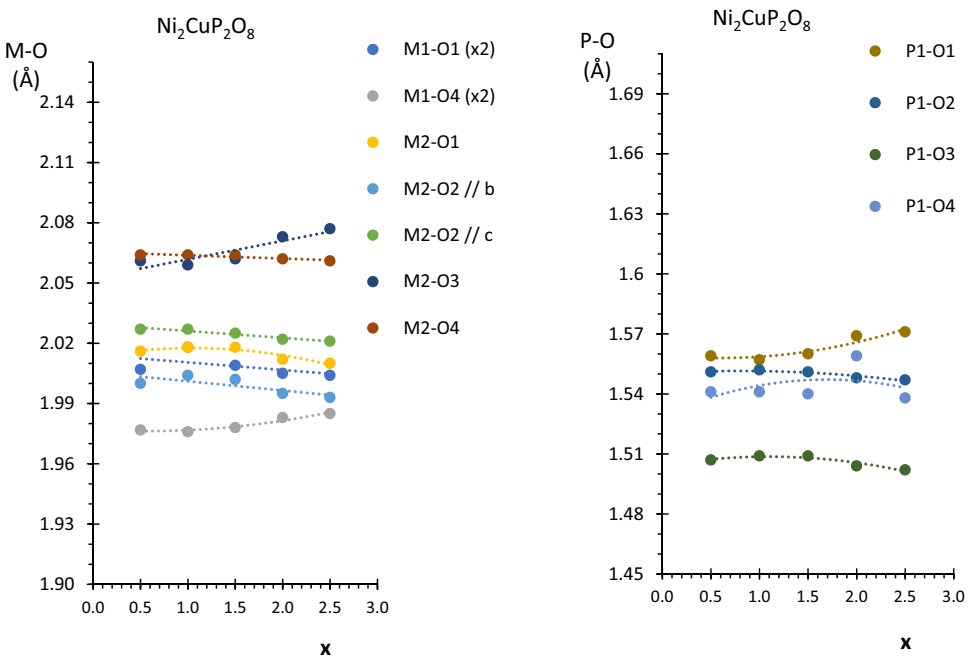

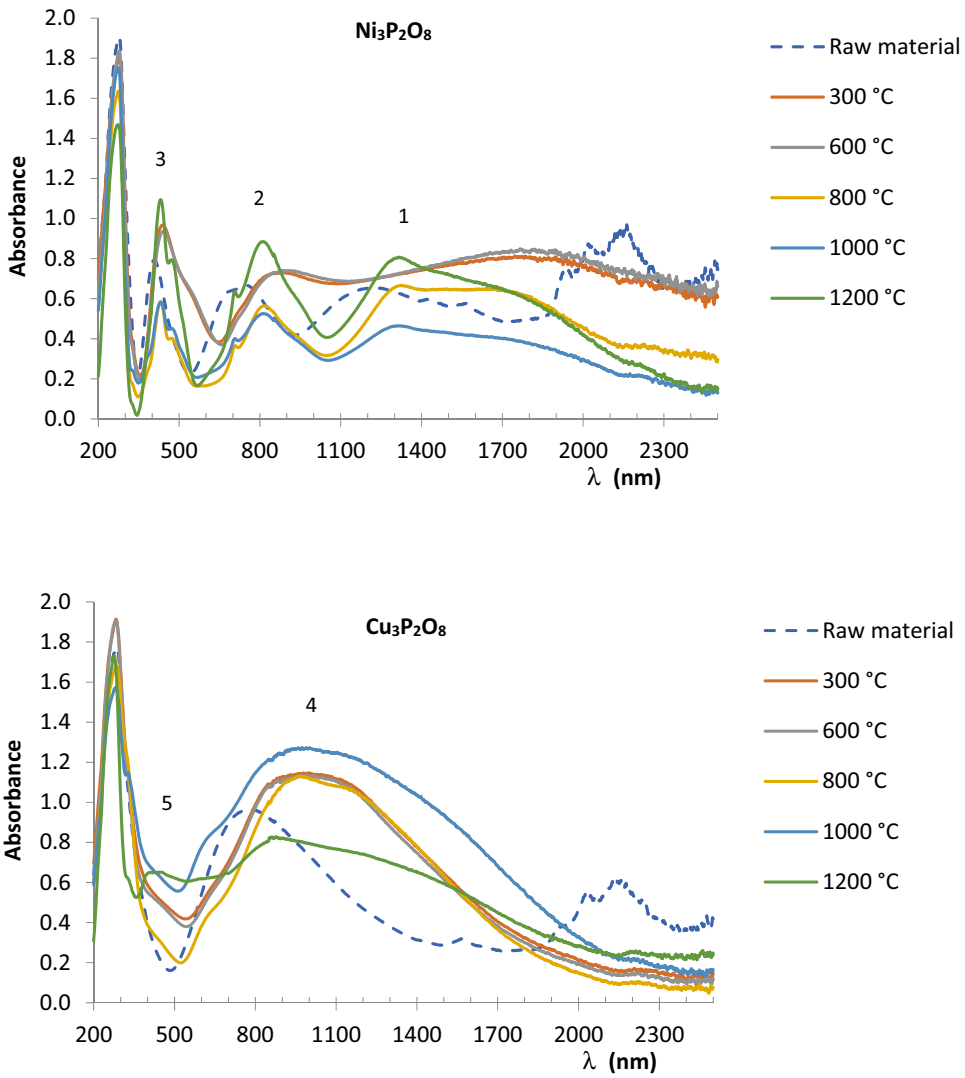

Fig. 9 UV–vis–NIR spectra of $Ni_3P_2O_8$ ($x = 0.0$) and $Cu_3P_2O_8$ ($x = 3.0$) compounds. Ni^{2+} in CN = 6: (1) $^3A_2 \rightarrow {}^3T_2(F)$, (2) $^3A_2 \rightarrow {}^3T_1(F)$, (3) $^3A_2 \rightarrow {}^3T_1(P)$ and charge transfer band. Cu^{2+} in CN = 4 and 5: (4) d-d transition (d^9 ion), (5) charge transfer band

difficult to distinguish the first and second Ni(II) transition bands. The lower definition of the absorption bands at $T \geq 1000$ °C modifies the colouration of the samples.

Figure 11 and Table 6 show the observed colour of the compositions at 70, 600, 800, 1000 and 1200 °C. The yellowish green ($x = 0.0$), bluish green ($x = 0.5$) and light blue colouration ($1.0 \leq x \leq 3.0$) of the materials at 25 °C changes to yellow ($0.0 \leq x \leq 2.0$), pale green ($x = 2.5$) and bluish green ($x = 3.0$) at 800 °C. The $Ni_3P_2O_8$ ($0.0 \leq x \leq 1.0$), $Ni_2CuP_2O_8$ ($0.5 \leq x \leq 2.5$) and $Cu_3P_2O_8$ ($2.5 \leq x \leq 3.0$) crystalline phases were detected at this temperature. Thus, the main change in colour with increasing Cu(II) in the samples is detected together with the presence of the $Cu_3P_2O_8$ structure at 800 °C. Yellow colouration is also obtained in $0.0 \leq x \leq 1.0$ compositions at 1000 °C. Brown colouration in $x = 1.5$ at 1000 °C (not obtained at 800 °C) and in $x = 1.0$ or 2.0 at 1200 or beige colouration in $x = 0.5$ at 1200 °C is associated with the lower definition of the Ni(II) transition bands and can be related to the observed structural distortion when solid solutions

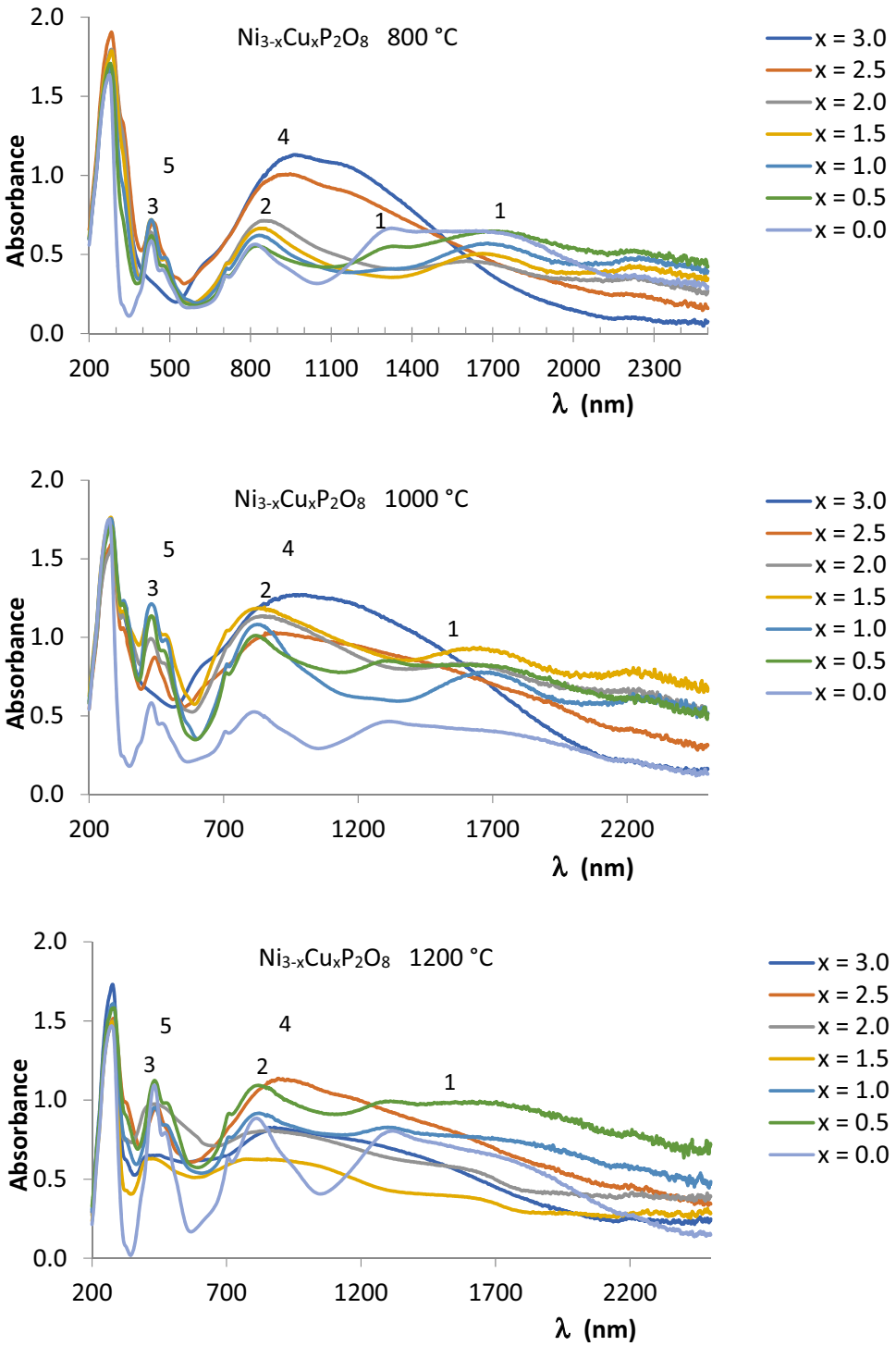

Fig. 10 UV–vis–NIR spectra of $Ni_{3-x}Cu_xP_2O_8$ ($0.0 \le x \le 3.0$) compositions. Ni^{2+} in CN = 6: (1) $^3A_2 \rightarrow {}^3T_2(F)$, (2) $^3A_2 \rightarrow {}^3T_1(F)$, (3) $^3A_2 \rightarrow {}^3T_1(P)$ and charge transfer band. Cu^{2+} in CN = 4 and 5: (4) d-d transition (d^9 ion), (5) charge transfer band

are formed or to the presence a different crystal structure. Both circumstances produce changes in the M–O (M = Cu, Ni) interatomic distances and the position of the bands in the spectra. The formation of solid solutions with presence of a small amount of Cu(II) in $Ni_3P_2O_8$ structure modifies the colour of the material from yellow to beige. At 1200 °C, the change from yellow ($x = 0.0$) to beige-brown is obtained when the diffraction intensity of $Ni_3P_2O_8$ crystalline phase is strong (Table 1) and the $Ni_{3-x}Cu_xP_2O_8$ ($0.0 \le x \le 0.7$) solid solutions with this

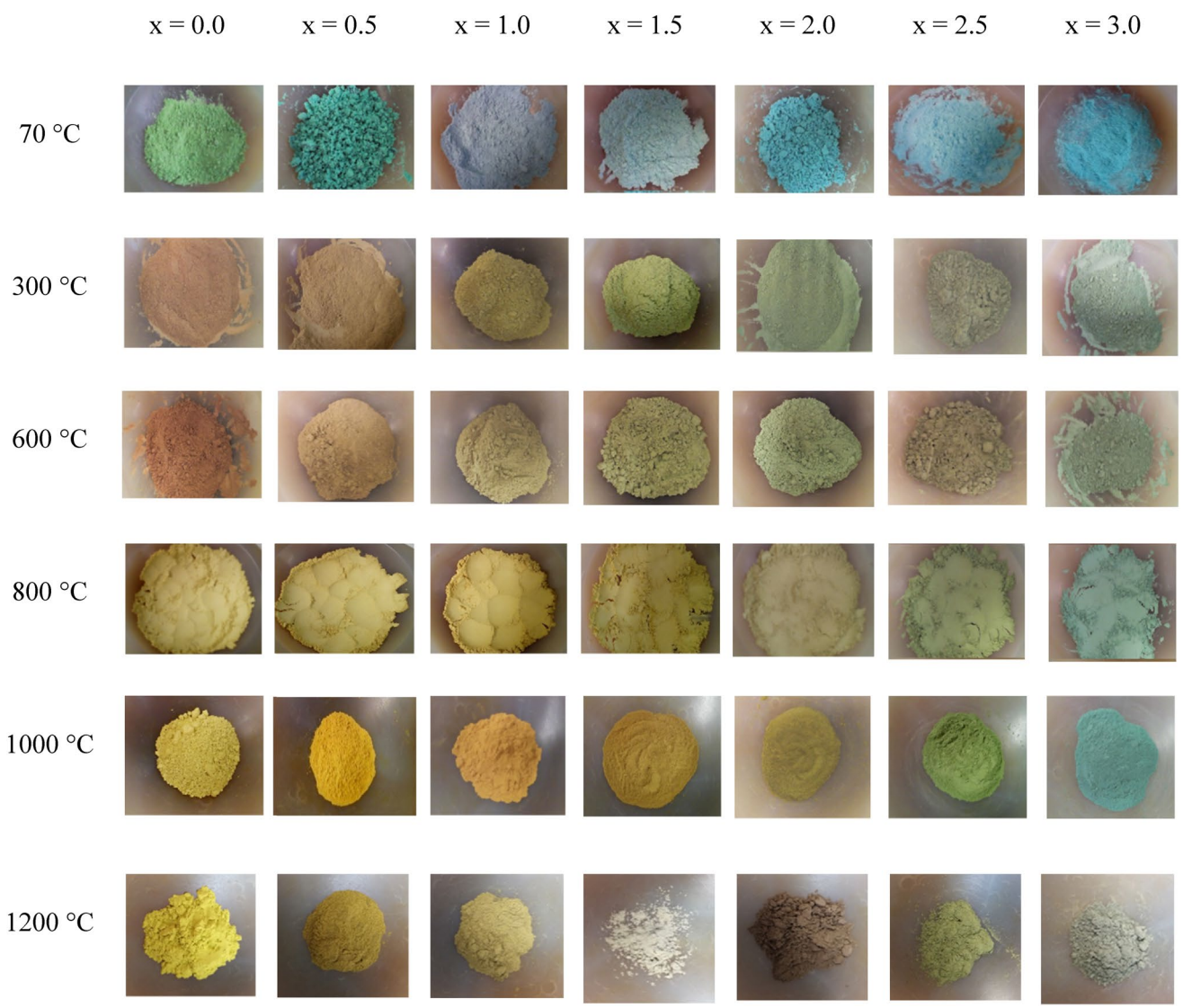

Fig. 11 The colour images of all the as-prepared samples (dried and fired $Ni_{3-x}Cu_xP_2O_8$ $0.0 \le x \le 3.00$ compositions)

structure are stable (Fig. 5). Because of this stability at the work temperature in the ceramic industry (the $Ni_3P_2O_8$ compound melts at 1350 °C), these materials may be used as ceramic pigments.

4 Conclusions

$Ni_{3-x}Cu_xP_2O_8$ ($0.0 \le x \le 3.0$) compositions were synthesized via the chemical co-precipitation method. Structural characterization of these materials and the variation in the unit cell parameters with composition in $Ni_3P_2O_8$, $Ni_2CuP_2O_8$ and $Cu_3P_2O_8$ structures confirm the formation of solid solutions in these structures in a partial compositional range. Between 800 and 1200 °C, $Ni_{3-x}Cu_xP_2O_8$ solid solutions with a $Ni_3P_2O_8$ structure were formed when $x \le 0.7$. $Ni_{3-x}Cu_xP_2O_8$ solid solutions with the $Ni_2CuP_2O_8$ structure were formed when $1.0 \le x \le 2.5$ at 800 and 1000 °C. At T > 600 °C, the $Cu_3P_2O_8$ structure is developed in the compositions with $x \ge 2.5$. The variation in volume with x in these structures is slight. The variation in the unit cell parameters in the same structure is the opposite because of structural distortion with inverse variation in the interatomic distances. These structures are not compact throughout their volume; they include less dense areas that allow their deformation.

Table 6 CIE L* a* b* colour parameters and observed colour in $Ni_{3-x}Cu_xP_2O_8$ $0.0 \le x \le 3.00$ compositions

T (°C)	*x*	*L**	*a**	*b**	Observed colour
70	0.0	76.44	−20.66	+24.86	Yellowish green
70	0.5	52.66	−29.10	−1.34	Bluish green
70	1.0	69.94	−8.41	−9.53	Light blue
70	1.5	79.96	−10.72	−3.55	Light blue
70	2.0	65.53	−19.19	−10.80	Light blue
70	2.5	79.45	−15.80	−8.99	Light blue
70	3.0	74.13	−22.52	−11.87	Light blue
600	0.0	59.29	+10.97	+24.21	Reddish beige
600	0.5	63.29	+2.87	+22.16	Beige
600	1.0	70.51	−2.28	+22.43	Yellowish green-beige
600	1.5	75.53	−7.05	+17.68	Yellowish green
600	2.0	77.22	−10.15	+15.44	Light green
600	2.5	60.64	−2.87	+13.20	Green–brown
600	3.0	69.46	−8.68	+7.92	Bluish green
800	0.0	82.75	−1.02	+27.94	Yellow
800	0.5	8.19	+0.06	+29.09	Yellow
800	1.0	79.36	+0.23	+32.89	Yellow
800	1.5	80.09	−2.75	+33.72	Yellow
800	2.0	80.65	−3.61	+29.48	Yellow
800	2.5	72.87	−9.30	+23.57	Pale green
800	3.0	78.53	−16.23	+4.35	Bluish green
1000	0.0	82.38	−1.22	+35.47	Yellow
1000	0.5	65.04	+7.04	+46.62	Yellow
1000	1.0	62.43	+10.53	+48.60	Yellow
1000	1.5	52.30	+3.71	+29.80	Brown
1000	2.0	58.47	−2.88	+27.39	Yellowish green
1000	2.5	56.30	−8.80	+19.56	Green
1000	3.0	56.74	−12.97	-0.28	Bluish green
1200	0.0	78.90	+4.92	+56.89	Yellow
1200	0.5	58.31	+6.43	+30.34	Beige
1200	1.0	60.20	+5.96	+24.86	Brown
1200	1.5	62.11	+1.26	+10.47	Grey
1200	2.0	49.97	+7.27	+14.04	Brown
1200	2.5	57.87	−0.32	+21.04	Green
1200	3.0	52.27	+0.42	+7.17	Dark greyish green

A gradual change from yellow to brown is obtained when the $Ni_3P_2O_8$ crystalline phase is obtained with a strong diffraction intensity ($0.0 \le x \le 1.0$) at 1200 °C. These compositions are yellow at 800 and 1000 °C. Under the conditions employed in this study, the broadest compositional range ($0.0 \le x \le 2.0$) within which the materials are yellow is obtained at 800 °C. At this temperature, yellow materials are obtained from $Ni_{3-x}Cu_xP_2O_8$ solid solutions with a $Ni_3P_2O_8$ or $Ni_2CuP_2O_8$ structure. $Ni_{3-x}Cu_xP_2O_8$ ($0.0 \le x \le 0.7$) yellow–brown solid solutions with $Ni_3P_2O_8$ structure are stable at 1200 °C and may be used as ceramic pigments.

Acknowledgements We gratefully acknowledge the financial support provided by Spain's Ministerio de Ciencia, Innovación y Universidades, Project MAT2016-78155-C2-1-R.

Compliance with ethical standards

Conflict of interest The authors declare that they have no conflict of interest.

References

1. Zhao W, Zhong G, Jian Z, Jianming Z, Song J, Gong Z, Chen Z, Zheng G, Jiang Z, Yang S (2018) Insights into the electrochemical reaction mechanism of a novel cathode material $CuNi_2(PO_4)_2$/C for Li-ion batteries. ACS Appl Mater Interfaces 10:3522–3529. https://doi.org/10.1021/acsami.7b15086
2. Zhong G, Bai J, Duchesne PN, McDonald MJ, Li Q, Hou X, Tang JA, Wang Y, Zhao W, Gong Z, Zhang P, Fu R (2015) Copper phosphate as a cathode material for rechargeable Li batteries and its electrochemical reaction mechanism. Chem Mater 27:5736–5744. https://doi.org/10.1021/acs.chemmater.5b02290
3. Escobal J, Pizarro JL, Mesa JL, Rojo JM, Bazan B, Arriortua MI, Rojo T (2005) Neutron diffraction, specific heat and magnetic susceptibility of $Ni_3(PO_4)_2$. J Solid State Chem 178:2626–2634. https://doi.org/10.1016/j.jssc.2005.06.022
4. Tena MA, Mendoza R, García JR, García-Granda S (2017) Structural characterization and colour of $Ni_3V_xP_{2-x}O_8$ ($0 \le x \le 2$) and $Ni_2V_yP_{2-y}O_7$ ($0 \le y \le 2$) materials. Results in Physics 7:1095–1105. https://doi.org/10.1016/j.rinp.2017.02.021
5. Tena MA, Mendoza R, Trobajo C, García JR, García-Granda S (2018) $Co_2P_2O_7$–$Ni_2P_2O_7$ solid solutions: Structural characterization and color. J Am Ceram Soc 00:1–10. https://doi.org/10.1111/jace.16158
6. Tena MA, Mendoza R, Martinez D, Trobajo C, García JR, García-Granda S (2020) Characterization of yellow and red inorganic pigments from $Mg_{0.5}Cu_{1.5}V_xP_{2-x}O7$ ($0 \le x \le 2$) solid solutions. SN Appl Sci 2:1–10. https://doi.org/10.1007/s42452-020-2917-7
7. Weimann I, Feller J, Žak Z (2017) Phase equilibria in the system CuO–NiO–P4O10 and synthesis, crystal structure, and characterization of the new copper nickel oxide phosphate $Cu_3NiO(PO_4)_2$. Z Anorg Allg Chem 643:299–305. https://doi.org/10.1002/zaac.201600403
8. Calvo C, Faggiani R (1975) Structure of nickel orthophosphate. Can J Chem 53:1516–1520. https://doi.org/10.1139/v75-210
9. Inorganic Crystal Structure Database (ICSD web). Fachinformationszentrum (FIZ, Karlsruhe, Germany).
10. Rietveld HM (1969) A profile refinement method for nuclear and magnetic structures. J Appl Crystallogr 2:65–71. https://doi.org/10.1107/S0021889869006558

11. Rodriguez-Carvajal J (September 2018-ILL-JRC), Fullprof.2k computer program, version 6.50, France.
12. Chapon L (Rutherford Appleton Laboratory, UK) and Rodriguez-Carvajal J (Institut Laue Langevin, France) (August 2008). FPStudio computer program, version 2.0
13. Goñi A, Lezama L, Pizarro JL, Escobal J, Arriortua MI, Rojo T (1999) Intercalation of Cu^{2+} in the $HNiPO_4{\cdot}H_2O$ layered phosphate: study of the structure, spectroscopic, and magnetic properties of the intercalated derivative and the related $CuNi_2(PO_4)_2$ compound. Chem Mater 11:1752–1759. https://doi.org/10.1021/cm980785w
14. Escobal J, Pizarro JL, Mesa JL, Larrañaga A, Rodriguez Fernandez J, Arriortua MI, Rojo T (2006) Magnetic susceptibility, specific heat and magnetic structure of $CuNi_2(PO_4)_2$. J Solid State Chem 179:3052–3058. https://doi.org/10.1016/j.jssc.2006.05.034
15. Forsyth JB, Wilkinson C, Paster S, Effenberger H (1990) The antiferromagnetic structure of triclinic copper(II) phosphate. J. Phys.: Condens. Matter 2:1609–1617. https://doi.org/10.1088/0953-8984/2/6/019
16. Shvanskaya LV, Volkova OS, Vasiliev AN (2020) A review on crystal structure and properties of 3d transition metal (II) orthophosphates $M_3(PO_4)_2$. J Alloy Compd 835(155028):1–4. https://doi.org/10.1016/j.jallcom.2020.155028
17. Tena MA (2012) Characterization of $Mg_xM_{2-x}P_2O_7$ (M = Cu and Ni) solid solutions. J Eur Ceram Soc 32:389–397. https://doi.org/10.1016/j.jeurceramsoc.2011.09.018
18. Commission Internationale del'Eclairage (1971) In: Recommendations on Uniform Color Spaces, Color Difference Equations, Phychometrics Color Terms. 1978. Supplement No. 2 of CIE Publication No. 15 (E1–1.31). Bureau Central de la CIE, Paris.
19. Lever ABP (1977) Inorganic electronic spectroscopy (second edition). Elsevier, Amsterdam, pp 507–511